GSI

GSI-Preprint-97-07
Januar 1997

BETA-DECAY STUDIES OF ^{107}Sb AND OTHER NEUTRON-DEFICIENT ANTIMONY ISOTOPES

M. Shibata, Z. Hu, J. Agramunt, D. Cano-Ott, R. Collatz, M. Górska, H. Grawe, M. Hellström, Z. Janas, M. Karny, R. Kirchner, O. Klepper, A. Plochocki, E. Roeckl, K. Rykaczewski, K. Schmidt, A. Weber, J Zylicz

(To be published in Phys. Rev. C)

Gesellschaft für Schwerionenforschung mbH
Planckstraße 1 • D-64291 Darmstadt • Germany
Postfach 11 05 52 • D-64220 Darmstadt • Germany

Beta-decay studies of ^{107}Sb and other neutron-deficient antimony isotopes

M. Shibata[1], Z. Hu[1], J. Agramunt[2], D. Cano-Ott[2], R. Collatz[1], M. Górska[1,3], H. Grawe[1], M. Hellström[1], Z. Janas[3], M. Karny[3], R. Kirchner[1], O. Klepper[1], A. Płochocki[3], E. Roeckl[1], K. Rykaczewski[3], K. Schmidt[1], A. Weber[1], J. Żylicz[3]

[1] *Gesellschaft für Schwerionenforschung, D-64291 Darmstadt, Germany*

[2] *Instituto de Física Corpuscular, E-46100 Burjassot Valencia, Spain*

[3] *Institute of Experimental Physics, University of Warsaw, PL-00681 Warsaw, Poland*

(January 15, 1997)

Abstract

By using on-line mass separation of residues from heavy-ion induced fusion-evaporation reactions, we studied the β^+/EC decay of the neutron-deficient isotopes ^{107}Sb and ^{108}Sb. A search for direct proton decay of ^{105}Sb did not yield a conclusive result. The experimental beta-decay half-lives of $^{104-108}$Sb are discussed with reference to results obtained from quasi-particle random-phase approximations, while the ^{108}Sb$\rightarrow$^{108}Sn and ^{107}Sb$\rightarrow$^{107}Sn level schemes are interpreted in comparison with shell model predictions.

23.40.-s; 23.50.+z; 27.60.+j

I. INTRODUCTION

Very neutron-deficient isotopes near the doubly closed-shell nucleus ^{100}Sn have attracted considerable interest recently as they are characterized by unique nuclear-structure features such as, *e.g.*, the occurrence of fast $\pi g_{9/2} \rightarrow \nu g_{7/2}$ GT beta-decays as well as proton, alpha and maybe even cluster radioactivity [1]. The experimental progress in this field includes the identification of ^{100}Sn and neighbouring isotopes [2,3], the measurement of the mass of ^{100}Sn and ^{100}In [4], in-beam spectroscopy of ^{99}Cd [5], observation of proton radioactivity for ^{105}Sb [6] and ^{112}Cs [7], and beta-decay studies of ^{94}Ag [8], $^{100-104}$In [9] and ^{101}Sn [10].

In this paper we want to report on an investigation of very neutron-deficient isotopes of antimony (Z=51), performed by using the GSI on-line mass separator. After describing the related experimental techniques in Sec. II, we present in Sec. III the results obtained for the β^+/EC decay of ^{108}Sb and ^{107}Sb as well as those deduced from a search for β^+/EC decay of ^{106}Sb and for proton radioactivity of ^{105}Sb. In Sec. IV, the experimental results are compared with model predictions. The β-decay half-lives as gross properties are compared to the results of a quasi-particle random-phase approximation, that uses decay energies and different decay modes obtained from global fits of the model parameters [11]. The detailed level schemes of the decay daughters and their feeding pattern are discussed within the spherical shell model, using a ^{100}Sn core and the full neutron $d_{5/2}$, $g_{7/2}$, $s_{1/2}$, $d_{3/2}$, and $h_{11/2}$ shells [12,13]. Sec. V contains a summary and an outlook.

II. EXPERIMENTAL TECHNIQUES

The neutron-deficient antimony isotopes of interest were produced by fusion-evaporation reactions induced by a ^{58}Ni beam from the UNILAC on isotopically enriched ^{50}Cr, ^{52}Cr and ^{58}Ni targets. The chromium targets were supported by molybdenum backings. For the measurements of decay properties, performed at the GSI on-line mass separator, a FEBIAD-E ion source [14] was used. This ion source was altered compared to its original version: a

modified anode cylinder permitted the use of very thin (4 mg/cm^2) tantalum catcher foils, and the inner surfaces of the source electrodes were coated with pyrolytic graphite. The latter measure turned out to double the effusion speed for antimony as determined from a separate test measurement of the half-life dependence of the separation efficiency by means of the implantation technique [15]. The result shown in Fig. 1 actually gives the lower limit of the total separation efficiency for antimony; several improvements in the main experiment as compared to the test, which tend to increase the efficiency (by a factor of the order of 2-3 for short-lived isotopes), could not be quantified and are thus not considered in Fig. 1.

The mass-separated beam was implanted into a tape, which periodically moved into a counting position equipped with a low-energy germanium detector and a large volume germanium detector. Alternatively the mass-separated beam was stopped in thin carbon foils mounted in front of two ΔE-E silicon detector telescopes, the beam being switched periodically between these foils. Low energy protons were searched in the ΔE spectra accumulated in anticoincidence with signals from the E detectors. Table I compiles the experimental parameters relevant for these measurements.

III. RESULTS

Figs. 2 and 3 show examples of the γ-ray spectra measured in this work for the decays of ^{108}Sb and ^{107}Sb. The corresponding experimental data are compiled in Tables II and III, respectively. The γ-ray energies have been determined on the basis of a calibration performed by means of standard sources before and after the on-line measurements. This calibration also reproduces the energies of the known β-delayed γ-lines from the decay of ^{108}Sn [17] and ^{107}Sn [18]. These activities represent the dominant contaminants of the A=108 and A=107 spectra, respectively (see Figs. 2 and 3). As only partial decay schemes and spin/parity assignments have been obtained, the γ-ray intensities given in Tables II and III have *not* been corrected for summing effects and conversion.

Concerning half-life determination, isotope identification and γ-ray assignments, the fol-

lowing procedure has been chosen. Firstly, the half-lives of ^{108}Sb and ^{107}Sb were deduced from the time characteristics of those γ-lines that can unambiguously be assigned on the basis of coincidence relations with Sn KX-rays and 511 keV quanta to be EC/β^+-delayed radiation from the decay of antimony isotopes. These conditions are fulfilled for the 253, 905, 1206 and 1273 keV γ-lines in the A=108 spectrum, and for the 151 keV γ-line in the A=107 spectrum. In addition, the Sn K_α line was used for the determination of the half-life of ^{108}Sb. The data, listed in Tables II and III and displayed in Figs. 4 and 5, yield half-life values of 7.6(3) s for ^{108}Sb and 4.6(8) s for ^{107}Sb. Additional γ-rays with consistent time characteristics were assigned to the respective decays. Compared to reference [17], the β-decay scheme of ^{108}Sb has been extended by 14 new γ-ray transitions. The 16 γ lines known for this decay have been placed in the level scheme shown in Fig. 6, establishing 9 new levels. In the β decay of ^{107}Sb, which was studied for the first time, four γ-ray transitions were found. Preliminary results of this work were already presented in the 1981 edition of the Karlsruhe Chart of Nuclides [19] as well as in its 1995 edition [20]; the 1454 keV line given there is, however, not confirmed in this final analysis. Due to low coincidence efficiency and missing cross-over transitions, only two γ-rays have been placed in the level scheme displayed in Fig. 7.

The search for β-delayed γ-rays of ^{106}Sb remained unsuccessful. The ^{106}Sb activity is evidently too weak to be observed in the presence of the isobaric contaminant ^{106}Sn and the room background. Assumming the known 1208 keV $2_1^+ \rightarrow 0^+$ transition in ^{106}Sn [21] to be populated with a branching ratio of 100% in the β decay of ^{106}Sb, the corresponding upper limits for source strength and production cross-section are 2 atoms/s·10 part·nA and 100 μb, respectively.

The search for direct proton decay of ^{105}Sb yielded the result displayed in Fig. 8. The proton energy-loss events, stemming from the known β-delayed proton decay of the daughter isotope ^{105}Sn [22], are almost quantitatively supressed by the anticoincidence condition. Therefore, the low-energy tail in the spectra shown in Fig. 8 is essentially due to positron energy-loss events.

IV. DISCUSSION

A. Direct proton decay of ^{105}Sb

The data shown in Fig. 8 do not yield clear evidence for the occurence of the 478 ± 15 keV proton line observed by Tighe *et al.* [6]. The weak indication of some excess events around proton energies of 500 keV would roughly correspond to the rate expected from the Berkeley experiment. This conclusion is based on the figures of merit (or sensitivities) of the two measurements as compiled in Table IV. Since the production cross section of the ^{50}Cr(^{58}Ni, p2n) reaction is unknown, these experiments do not allow to determine a (limit for the) branching ratio for direct proton decay of ^{105}Sb. In a recent measurement performed at the projectile fragment separator (FRS) of GSI, Friese *et al.* [23] found a value of ≈1% for this quantity, based on the observation of one event with a proton energy of 550 ± 30 keV. Due to insufficient statistics and energy resolution, our data do not enable us to make a firm statement concerning the 2σ discrepancy between the proton energies measured by Tighe *et al.* and Friese *et al.*, respectively.

B. β-decay half-lives for $^{103-108}$Sb

Table V compares data for antimony isotopes, compiled either from measurements or from systematic trends, to results from calculations obtained from a quasi-particle random-phase approximation (QRPA) [11] and a proton-neutron quasi-particle random-phase approximation (pn-QRPA) [29]. The model parameters used in Ref. [11] result from a global fit to nuclei ranging from ^{16}O to the heaviest known nuclei. As can be seen from the values compiled in Table V, this model seems to systematically underestimate the experimental half-lives by a factor of 2.5 - 5. In the calculation of the total *ft* value, derived from the summed calculated GT strength $\Sigma B(GT)$, a coupling constant $B = 6160/(g_A/g_V)^2 = 4131s$ was used in Ref. [11], which does not include any quenching of the GT strength. The reduction factors compare well with observed GT hindrance in this region of nuclei [30]. However,

in the *global* comparison of QRPA β half-lives with experiment there is no indication for a general reduction of the GT strength [11]. On the other hand, the pn-QRPA predictions [29] seem to overestimate the experimental half-lives by factors of 1.4 - 3.4. The difference in the two theoretical approaches is due to the different treatment of the GT interaction $V_{GT} = 2x \sum_i \sigma_i t_i^+$. Möller *et al.* [11] treat particle-hole (ph) correlations only with a global strength $x = 23/A$ MeV, whereas Hirsch *et al.* [29] regard also particle-particle (pp) correlation, fitting the corresponding strength parameters separately to known beta-decay half-lives in each isotopic chain. A more detailed discussion of the β decay half-lives of light antimony isotopes would require a detailed knowledge of the GT distribution, which is not available.

C. β-decay schemes of ^{107,108}Sb

1. Shell model calculations

We have performed shell model calculations for light tin isotopes in the $1d_{5/2}$, $1g_{7/2}$, $2s_{1/2}$, $1d_{3/2}$, $0h_{11/2}$ neutron space, using a ^{100}Sn core. Details of the calculations are given in Refs. [12,13]. As this is part of a series of shell model calculations in the "triangle" ^{90}Zr-^{100}Sn-^{108}Sn, no attempt has been made to specifically adjust single particle energies and two-body matrix elements (TBME) to ^{107,108}Sn. The nucleon-nucleon ($\nu\nu$) interaction was obtained from a realistic set of TBME, derived by renormalization from nucleon-nucleon scattering data [33] and, when the $\nu h_{11/2}$ orbital is involved, from the Kuo-Herling set in ^{208}Pb [34], by replacing (n, l, j) by (n, l+1, j+1) [33] and scaling with 1/A. GT transition strengths were estimated by assuming pure $\pi d_{5/2}$ and $(\pi d_{5/2} \nu d_{5/2})_{4+}$ configurations for the ^{107,108}Sb ground states, respectively.

2. β-decay scheme of ^{108}Sb

The low statistics of the experimental data only allowed to establish coincidence relations for a few of the γ-rays assigned to the decay of ^{108}Sb. Therefore, the experimental decay

scheme of this nucleus, shown in Fig. 6, was deduced from the list of γ-rays, given in Table II, on the basis of the following arguments:

- The lowest $I^\pi = 2^+$, 4^+, 6^+ levels and the connecting 1206, 905 and 253 keV γ-rays are known from in-beam experiments [17], and are corroborated by the coincidence relations determined in the present work.

- From γ-ray energy sums and differences, the γ-lines of 491, 530, 744, 821, 865, 949, 1434, 1649, 1770 and 2154 keV can be combined with known levels and transitions, establishing new levels at excitation energies E_x = 2154, 2640, 2855 and 2976 keV.

- The remaining high energy γ-rays of 1273, 1599 and 1869 keV are assigned to γ-transitions between high-lying levels and the $I^\pi = 2^+$ state at E_x = 1206 keV. The assignment is based on the most probable assumption that the GT decay proceeds via $\pi d_{5/2} \rightarrow \nu d_{3/2}$ or $\pi d_{5/2} \rightarrow \nu d_{5/2}$ followed by strong spin-flip $\nu d_{3/2} \rightarrow \nu d_{5/2}$ and diagonal $\nu d_{5/2} \rightarrow \nu d_{5/2}$ M1 decay with the maximum possible γ-transition energy to the $I^\pi = 2^+$ state. A direct γ-feeding of the $I^\pi = 0^+$ ground state conflicts with the probable parent spin $I^\pi = (4^+)$ (see below).

The γ decays of the E_x = 2976 and 2855 keV states limit their spins to $I^\pi = (3^+, 4^+)$ and (5^+), respectively. Since odd parity states are expected to lie at much higher excitation energies (see Fig. 6), $I^\pi = 4^+$ is the most probable assignment for the 2855 keV state. This yields $I^\pi = (4^+, 5^-)$ for the ^{108}Sb parent state, which leads to spins and parities of $I^\pi = (3, 4)^+$ for the remaining ^{108}Sn states fed in β^+/EC decay. The E_x = 2155 level can be assigned to be $I^\pi = (1^+, 2^+)$ from its γ-decay. This assignment is compatible with the energy-favoured very weak direct feeding of the $I^\pi = 2^+$ states. The general feeding pattern energetically resembles the β^+/EC decay of ^{110}Sb ($I^\pi = 3^+$) [16]. The main difference lies in the feeding of higher spin states in the ^{108}Sb decay, which corroborates the tentative level scheme and spin assignments.

In Fig. 6 we compare the tentative experimental ^{108}Sb$\rightarrow^{108}$Sn decay scheme with the results of shell model calculations. To demonstrate the quality of agreement, the shell model results are presented in four columns, one for selected states known from in-beam spectroscopy [34] and three for the lowest $I^\pi = 3^+, 4^+, 5^+$ states up to $E_x = 3.5$ MeV, respectively. As the level density of these states is very high (about 10 states between 2 and 3 MeV for each spin) only those levels are included whose leading configurations are likely to be fed in GT decay. The ^{108}Sb ground state has a dominant $(\pi d_{5/2}\nu d_{5/2}^{-1})_{4+}$ quasi-particle configuration with some admixture of $(\pi d_{5/2}\nu g_{7/2}^{-1})$. Therefore daughter states have been selected with leading configurations $(\nu d_{3/2}\nu d_{5/2}^{-1})_{3+,4+}$, $(\nu d_{5/2}^{-2})_{4+}$ and $(\nu d_{3/2}\nu g_{7/2})_{5+}$. It is obvious that the shell model accounts well for the number of states populated in β^+/EC decay between 2 and 3.5 MeV. In view of the tentative experimental level scheme we have refrained from calculating the theoretical GT distribution. As excitations of the Z=50 proton core were not regarded in the present shell model approach, GT decay to four-quasi-particle states of configuration $\pi d_{5/2}g_{9/2}^{-1}\nu d_{5/2}^{-1}g_{7/2}$ were not calculated. These states, which are expected at excitation energies above 4.0 MeV, are well within the Q_{EC} window but are characterized by even higher level density as compared to the energy range shown in Fig. 6. The γ-decay from these states would preferably populate low lying $I^\pi = 2^+$ states via E2 transitions, which would explain the weak feeding observed for the E_x=1206 and 2155 keV states.

3. β-decay scheme of ^{107}Sb

In this work, β-delayed γ-rays for ^{107}Sb were observed for the first time. From the γ-rays listed in Table III only the 151 keV γ-ray, which connects the $I^\pi = 7/2^+$ first excited state to the $I^\pi = 5/2^+$ ground state, is known from in-beam work [34]. In addition, the latter study succeeded in identifying several high-lying states in ^{107}Sn, which have been extended up to $I^\pi = 31/2^-$ in a recent study [35].

As argued in Sec. IV C 2, the GT decay of the light antimony isotopes proceeds prefer-

ably by the $\pi d_{5/2} \rightarrow \nu d_{3/2}$ and $\pi d_{5/2} \rightarrow \nu d_{5/2}$ transitions. The daughter $I^\pi = 3/2^+$ and $5/2^+$ states decay by allowed spin-flip or diagonal M1 transitions to the ^{107}Sn $I^\pi = 5/2^+$ ground state, which is the $\nu d_{5/2}$ single-particle state. We therefore assume that the observed high energy γ-transitions proceed directly to the ground state. In principle, a $d_{3/2} \rightarrow g_{7/2}$ stretched E2 transition to the $I^\pi = 7/2^+$ first excited state can not, for intensity reasons, be excluded for the 704 or 819 keV γ-lines. This would, however, require a B(E2) strength more than a factor of 10^3 higher than the allowed B(M1) strength, which is hard to conceive. (In this context, it should be noted that the states primarily fed in β^+/EC decay could be connected by competitive diagonal M1 transitions.) Thus we arrive at the tentative decay scheme and spin assignments $I^\pi = (3/2, 5/2, 7/2)^+$ shown in Fig. 7, which together with selected states from in-beam spectroscopy [34] are compared to the results of shell model calculations. A ^{106}Sn $0^+ \bigotimes \pi d_{5/2}$ configuration was assumed for the ^{107}Sb ground state; correspondingly, only $I^\pi = 3/2^+$ and $5/2^+$ states are expected to be populated in β^+/EC decay states. In Fig. 7 we have listed, together with the excitation energies calculated for the $3/2^+$ and $5/2^+$ levels, the ^{106}Sn $0^+ \bigotimes \nu d_{3/2}$ and $\nu d_{5/2}$ content for the $I^\pi = 3/2^+$, $5/2^+$ wave functions, which represent the GT distribution. (For comparable content of the respective configuration the $\pi d_{5/2} \rightarrow \nu d_{3/2}$ spin-flip GT decay is favoured by a geometrical factor of only 1.15 over the diagonal $\pi d_{5/2} \rightarrow \nu d_{5/2}$ GT transition.) For the most strongly fed state at $E_x = 1280$ keV, good agreement between shell model and experiment is observed. It should be noted, that this agreement yields the first evidence for the position of the $\nu d_{3/2}$ level in ^{101}Sn.

V. CONCLUSION

The use of fusion evaporation reactions in connection with on-line mass separation, and in particular the recent progress in ion-source development, have allowed us to observe β-delayed γ radiation of ^{107}Sb for the first time and to obtain improved β-decay data for ^{108}Sb. Even though the resulting experimental decay schemes of ^{107}Sb and ^{108}Sb are tentative and

incomplete, they allow a meaningful comparison with predictions obtained from shell-model calculations. The high level density of states populated in the GT decay of odd-even and odd-odd nuclei, as predicted by shell model calculations, strongly suggests the use of highly efficient arrays in future experiments, such as those based on high-resolution germanium detectors of the EUROBALL CLUSTER type [36] or low-resolution NaI total-absorption spectrometers. A prerequisite for such measurements is, however, the development of a chemically selective ion source for antimony isotopes, which is not available to date. An interesting alternative for continuing studies of low-spin states in the light tin isotopes is the determination of B(E2) values of the first excited state of neutron-deficient even-even tin isotopes by using Coulomb excitation of relativistic radioactive beams.

ACKNOWLEDGMENTS

The authors are indebted to K. Burkard and W. Hüller for continuous development of the separator and for its reliable operation. The excellent collaboration with the UNILAC operating group is gratefully acknowledged.

This work was supported in part by the European Community under Contract No. ERBCIPD-CT94-0091 and ERBFMGE-CT95-0083. The authors from Warsaw acknowledge support from the Polish Committee of Scientific Research (Grant No. KBN 2 P302 148 06). One of us (M. Hellström) would like to thank the Alexander von Humboldt-Foundation for support.

REFERENCES

[1] E. Roeckl, Nucl. Phys. **A583**, 849 (1995).

[2] R. Schneider, J. Friese, J. Reinhold, K. Zeitelhack, T. Faesterman, R. Gernhäuser, H. Gilg, F. Heine, J. Homolka, P. Kienle, H.J. Körner, H. Geissel, G. Münzenberg, and K. Sümmerer, Z. Phys. **A348**, 221 (1994).

[3] M. Lewitowicz, R. Anne, G.Auger, D. Bazin, C. Borcea, V. Borrel, J.M. Corre, M. Huyse, Z. Janas, H. Keller, S. Lukyanov, A.C. Mueller, Yu. Penionzhkevich, M. Pfützner, F. Pougheon, K. Rykaczewski, M.G. Saint-Laurent, K. Schmidt, W.D. Schmidt-Ott, O. Sorlin, J. Szerypo, O. Tarasov, J. Wauters, and J. Żylicz, Phys. Lett. **B332**, 20 (1994).

[4] M. Chartier, G. Auger, W. Mittig, A. Lepine-Szily, L. K. Fifield, J. M. Casandjian, M. Chabert, J. Ferme, A. Gillibert, M. Lewitowicz, M. Mac Cormick, M. H. Moscatello, O.H. Odland, N. A. Orr, G. Politi, C. Spitaels, and A. C. C. Villari, Phys. Rev. Lett. **77**, 2400 (1996).

[5] M. Lipoglavšek, J. Cedekäll, M. Palacz, J. Persson, A. Atac, J. Blomqvist, C. Fahlander, H. Grawe, A. Johnson, A. Kerek, W. Klamra, J. Kownacki, A. Likar, L.-O. Norlin, J. Nyberg, R. Schubart, D. Seweryniak, G. de Angelis, P. Bednarczyk, Zs. Dombrädi, D. Foltescu, D. Jerrestam, S. Juutinen, E. Mäkelä, G. Perez, M. de Poli, H. A. Roth, T. Shizuma, Ö. Skeppstedt, G. Sletten, S. Törmänen, and T. Vass, Phys. Rev. Lett. **76**, 888 (1996).

[6] R. J. Tighe, D. M. Moltz, J. C. Batchelder, T. J. Ognibene, M. W. Rowe, and Joseph Cerny, Phys. Rev. **C49**, R2871 (1994).

[7] R. D. Page, P. J. Woods, R. A. Cunningham, T. Davinson, N. J. Davis, A. N. James, K. Livingston, P. J. Sellin, and A. C. Shotter, Phys. Rev. Lett. **72**, 1798 (1994).

[8] K. Schmidt, Th.W. Elze, R. Grzywacz, Z. Janas, R. Kirchner, O. Klepper, A. Płochocki,

E. Roeckl, K. Rykaczewski, L.D. Skouras, and J. Szerypo, Z. Phys. **A350**, 99 (1994).

[9] J. Szerypo, M. Huyse, G. Reusen, P. Van Duppen, Z. Janas, H. Keller, R. Kirchner, O. Klepper, A. Piechaczek, E. Roeckl, D. Schardt, K. Schmidt, R. Grzywacz, M. Pfützner, A. Płochocki, K. Rykaczewski, J. Żylicz, G. Alkhazov, L. Batist, A. Bykov, V. Wittmann, and B. A. Brown, Nucl. Phys. **A584**, 221 (1995).

[10] Z. Janas, H. Keller, R. Kirchner, O. Klepper, A. Piechaczek, E. Roeckl, K. Schmidt, M. Huyse, J. von Schwarzenberg, J. Szerypo, P. Van Duppen, L. Vermeeren, F. Albus, H.-J. Kluge, G. Passler, F. P. Scheerer, N. Trautmann, V. N. Fedoseyev, V. I. Mishin, R. Grzywacz, A. Płochocki, K. Rykaczewski, and J. Żylicz, Physica Scripta **T56**, 262 (1995).

[11] P. Möller, J. R. Nix, and K.-L. Kratz, Atomic Data and Nuclear Data Tables, in print.

[12] H. Grawe, R. Schubart, K. H. Maier, and D. Seweryniak, Physica Script **T56**, 71 (1995).

[13] R. Schubart, H. Grawe, J. Heese, K. H. Maier, and M. Schramm, Z. Phys. **A352**, 373 (1995).

[14] R. Kirchner, Nucl. Instr. Meth. **186**, 295 (1981).

[15] R. Kirchner, Nucl. Instr. and Meth. **B70**, 186 (1992); GSI Sci. Rep. **96-1**, 173 (1996) and accepted for publication in Nucl. Instr. and Meth. **B** (1997).

[16] K. Oxorn, A. J. Houdayer, and S. K. Mark, Z. Phys. **A279**, 289 (1976).

[17] J. Blachot, Nuclear Data Sheet **62**, 803 (1991).

[18] J. Blachot, Nuclear Data Sheet **62**, 709 (1991).

[19] W. Seelmann-Eggebert, G. Pfennig, H. Müzel, and H. Klewe-Nebenius (eds.), Chart of Nuclides, 5th edition, Kernforschungszentrum Karsruhe (1981).

[20] G. Pfennig, H. Klewe-Nebenius, and W. Seelmann-Eggebert (eds.), Chart of Nuclides,

6th edition, Forschungszentrum Karlsruhe (1995).

[21] F. Azaiez, S. Andriamonje, J. F. Chemin, M. Fidah, J. N. Scheurer, M. M. Aléonard, G. Bastin, J. P. Thibaud, F. Beck, G. Costa, J. F. Bruandet, and F. Liatard, Nucl. Phys. **A501**, 401 (1989).

[22] P. Tidemand-Petersson, R. Kirchner, O. Klepper, W. Kurcewicz, E. Roeckl, and E. F. Zganjar, Z. Phys. **A302**, 343 (1981).

[23] J. Friese, Proceedings of the International Workshop XXIV on Gross Properties of Nuclei and Nuclear Excitations, Hirschegg, Austria, 123 (1996).

[24] P. Möller and J. R. Nix, Atomic Data and Nuclear Data Tables **26**, 165 (1981).

[25] A. H. Wapstra, G. Audi, and R. Hoekstra, Atomic Data and Nuclear Data Tables **39**, 281 (1988).

[26] G. Audi and A. H. Wapstra, Nucl. Phys. **A595**, 409 (1995).

[27] K. Rykaczewski, R. Anne, G. Auger, D. Bazin, C. Borcea, V. Borrel, J. M. Corre, T. Dörfler, A. Fomichov, R. Grzywacz, D. Guillemaud-Mueller, R. Hue, M. Huyse, Z. Janas, H. Keller, M. Lewitowicz, S. Lukyanov, A. C. Mueller, Yu. Penionzhkevich, M. Pfützner, F. Pougheon, M. G. Saint-Laurent, K. Schmidt, W. D. Schmidt-Ott, O. Sorlin, J. Szerypo, O. Tarasov, J. Wauters, and J. Żylicz, Phys. Rev. **C52**, R2310 (1995).

[28] M. Lewitowicz, in Proceedings of International Conference on Exotic Nuclei and Atomic Masses (ENAM 95), edited by M. de Saint-Simon and O. Sorlin (Edition Frontieres, Gif-sur-Yvette), 427 (1995).

[29] M. Hirsch, A. Staudt, K. Muto, and H. V. Klapdor-Kleingrothaus, Atomic Data and Nuclear Data Tables **53**, 165 (1993).

[30] A. Płochocki, K. Rykaczewski, T. Batsch, J.Szerypo, J. Żylicz, R. Barden, O. Klepper, E. Roeckl, D. Schardt, I. S. Grant, H. Grawe, P. Manakas, and L. D. Skouras, Z. Phys.

A342, 43 (1992).

[31] L. D. Skouras and C. Decles, Phys. Rev. **C15**, 1873 (1977).

[32] T. T. S. Kuo and G. H. Herling, Naval. Res. Lab., Washington, NRL Memorandum Report, 2258 (1971).

[33] G. A. Leander, J. Dudek, W. Nazarewicz, J. Nix, and P. H. Quentin, Phys. Rev. **C30**, 416 (1984).

[34] G. Auger, J. M. Lagrange, M. Pautrat, and J. Vanhorenbeeck, Nucl. Phys. **A426**, 109 (1984).

[35] T. Ishii, A. Makishima, K. Koganemaru, Y. Saito, M. Ogawa, and M. Ishii, Z. Phys. **A347**, 41 (1993).

[36] J. Eberth, in Proceedings of Conference on Physics from Large γ-Ray Detector Arrays, Berkeley, 1994, Report LBL-35687 1994, Vol. 2, p. 160.

TABLES

TABLE I. Parameters of the measurements.

Isotope	^{58}Ni Beam		Target		Detector	Measurement	Yield
	Energy (MeV/u)	Intensity (part.nA)	Isotopic abundance	Thickness (mg/cm^2)	Setup	Time (h)	$(\frac{atoms}{s \cdot 10 part.nA})$
^{108}Sb	5.0	~40	^{58}Ni 99.8%	3.8	[a] + [b]	0.5	150
^{107}Sb [e]	5.0	~16	^{58}Ni 99.9%	3.6	[c]	2	≥ 14
^{107}Sb	4.4	~40	^{50}Cr 92.6%	3.9	[a] + [b]	11	≥ 0.37
			^{52}Cr 6.9%				
^{106}Sb	4.7	~40	^{52}Cr 99.8%	3.7	[a] + [b]	2	< 2
^{105}Sb	5.3	~40	^{50}Cr 90.5%	3.9	[d]	11	?
			^{52}Cr 8.5%				
^{105}Sb	5.0	~40	^{50}Cr 96.2%	3.9	d	5	?
			^{52}Cr 3.6%				

[a]Low-energy germanium detector ($\phi 50.5 \times 20.0$) with the front surface of the detector ~5 mm away from the source.

[b]Large-volume high-purity germanium detector (21%) with the front surface of the detector ~5 mm away from the source.

[c]Large-volume high-purity germanium detector (23%) with the front surface of the detector ~3-5 mm away from the source.

[d]Two $\Delta E - E$ telescopes consisting of 20.3μm, 732μm and 15.6μm, 705μm detectors, respectively.

[e]Measurement made with an unmodified FEBIAD-E ion source containing a 0.2 mm thick graphite catcher [14].

TABLE II. Energies, relative intensities and coincidence relations of the γ-rays observed in the decay of ^{108}Sb.

	Present Work		Oxorn *et al.* [16]
E_γ(keV)	I_γ	coincident γ-rays (keV)	I_γ
253.3(2)	3.8(6)	Sn K_α, 511, 905, 1206	
490.7(3)	1.3(3)		
529.7(4)	1.2(2)		
744.0(3)	2.0(3)		
820.7(3)	5.0(8)		
865.0(3)	6.5(10)		
904.8(2)	26(4)	Sn K_α, 253, 511	24.9(80)
949.2(3)	5.3(9)		
1205.8(2)	100	Sn K_α, 253, 511	100
1272.9(3)	15(2)	Sn K_α, 511	
1434.4(4)	3.7(8)		
1598.5(3)	19(3)		
1648.6(4)	7.2(12)		
1769.7(5)	6.6(11)		
1868.7(5)	3.9(8)		
2154.4(5)	4.1(8)		

TABLE III. Energies, relative intensities and coincidence correlations of the γ-rays observed in the decay of ^{107}Sb.

E_γ(keV)	I_γ	coincident γ-rays (keV)
151.2(2)	45(8)	Sn K_α, 511
704.1(6)	28(7)	
819.4(6)	56(11)	
1280.1(3)	100	

TABLE IV. Comparison of the experimental parameters of the earlier ^{105}Sb experiment [6], performed at Berkeley, with those of this work. The relative figure of merit is defined to be the product of ^{58}Ni dose, target thickness, effective ^{50}Cr content of target, separation efficiency and detection efficiency, and is normalized to the parameters of the Berkeley experiment.

Parameter	Berkeley experiment	This work
^{58}Ni dose	$0.89 \cdot 10^{16}$	$1.4 \cdot 10^{16}$
Target thickness (mg/cm^2)	0.68	> 0.68 [a]
Effective ^{50}Cr content of target	0.56 [b]	> 0.63 [c]
Separation efficiency	0.02	> 0.01
Detection efficiency	0.16	0.16
Relative figure of merit	1	> 0.9

[a]The thickness of the chromium target is actually 3.9 mg/cm^2 (see Table I for the isotopic enrichments); the stated limit concedes that most of the (unknown) excitation function for the production cross-section may be already covered by 0.68 mg/cm^2

[b]Cr_2O_3 target, ^{50}Cr enrichment 96.8%.

[c]This lower limit concedes that our metallic ^{50}Cr target (enrichment 93.3% averaged) may have alloyed with the molybdenum backing during irradiation.

TABLE V. Compilation of decay data of antimony isotopes. The QRPA calculations of half-lives [11] were based on Q_{EC} values taken from the mass calculations of Möller *et al.* [24] (see column 2), while the pn-QRPA calculations of half-lives [29] used Q_{EC} values taken from the mass evaluations of Wapstra *et al.* [25] except for ^{103}Sb; in the latter case, the Q_{EC} value stems from the mass formula of Möller *et al.* [24] (see column 2). In column 4, we also list the Q_{EC} values taken from the most recent mass evaluation of Audi *et al.* [26] for comparison. Note that the Q_{EC} values from refs. [25] and [26] were derived at least partly from systematical trends.

Isotope	Q_{EC} (keV)			$T_{1/2}$(s)		
	[24]	[25]	[26]	experiment	QRPA [11]	pn-QRPA [29]
^{103}Sb	11840		11170(580)	> 1 μs [27]	0.092	0.262
^{104}Sb	13350	12300(830)	12200(390)	$0.44^{+0.15}_{-0.11}$ [23]	0.17	1.49
^{105}Sb	10290	9310(590)	9440(180)	1.12(16) [27]	0.32	1.68
^{106}Sb	11670	10930(500)	11070(310)	0.6(2) [28]	0.70	2.95
^{107}Sb	8530	7700(410)	7910(310)	4.6(8) [a]	1.36	10.4
^{108}Sb	10060	9540(300)	9490(210)	7.0(5) [15], 7.6(3) [a]	1.42	10.8

[a]from present work.

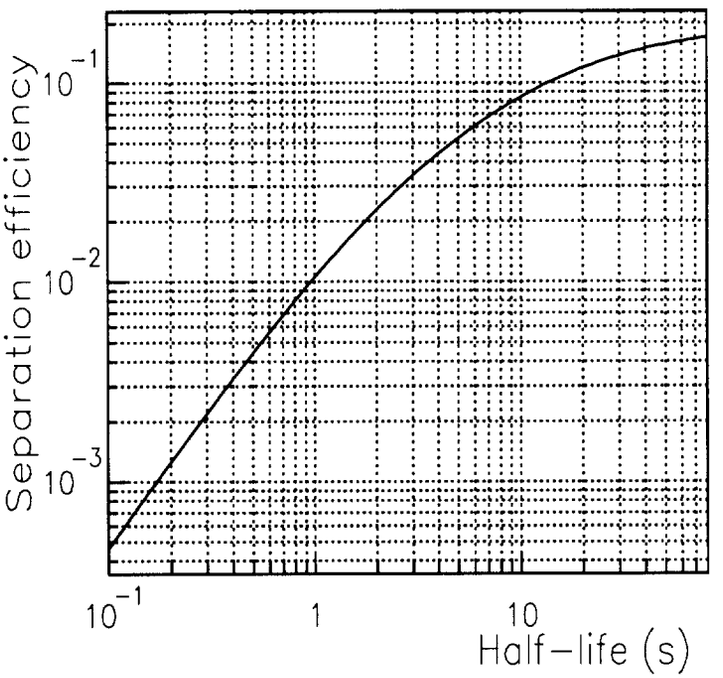

Figure 1: Lower limit of the separation efficiency as a function of half-life for antimony isotopes, considering all losses between production and detection.

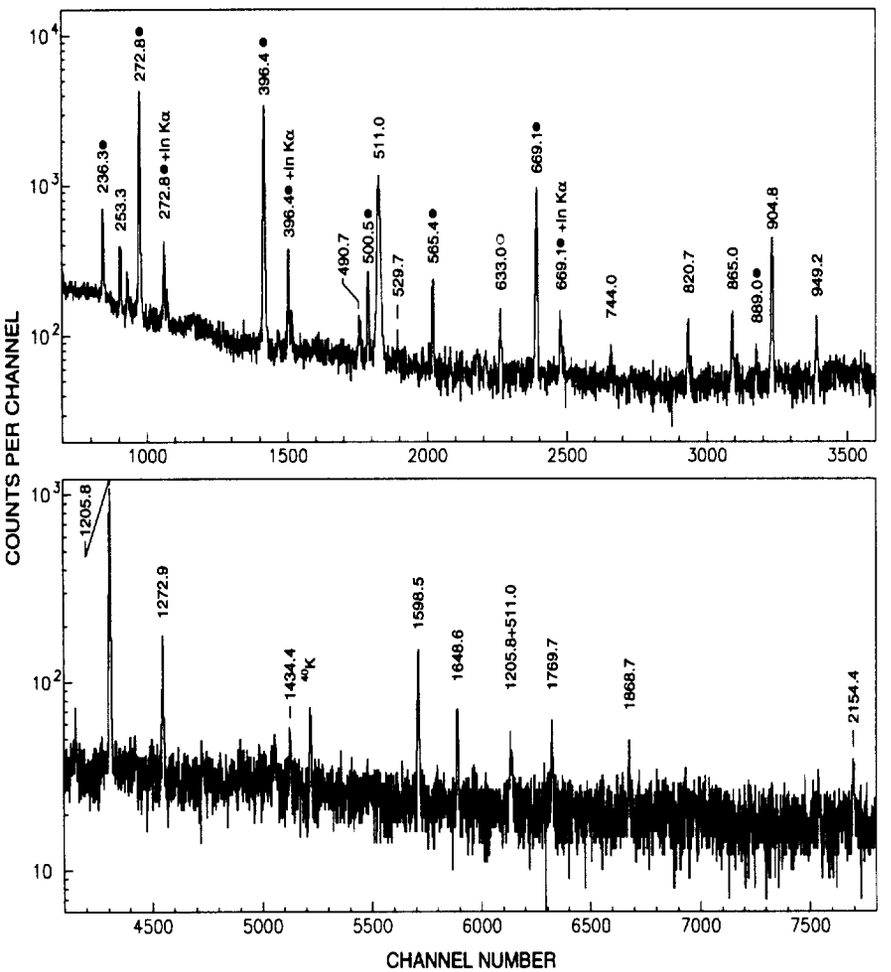

Figure 2: γ-ray singles spectrum from the β decay of ^{108}Sb obtained with the large-volume germanium detector. The γ lines are labeled with their energy in keV. The closed circles (•) indicate γ rays from the β decay of ^{108}Sn, the open circle (o) marks a γ ray from the β decay of ^{108}In. All other γ lines, except for the ^{40}K line, are assigned to the decay of ^{108}Sb.

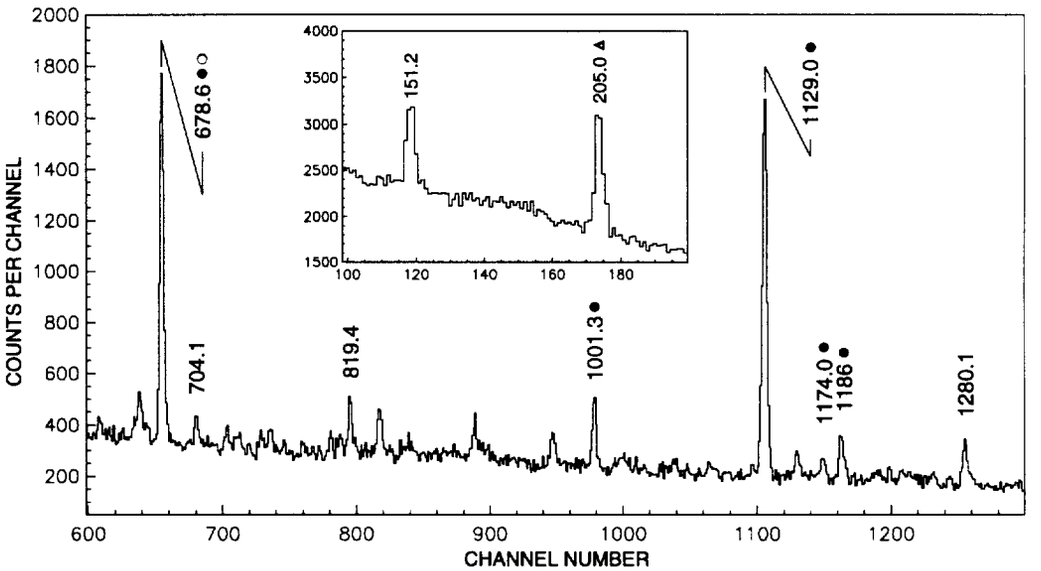

Figure 3: γ-ray singles spectrum from the β decay of ^{107}Sb obtained with the large-volume germanium detector. The γ lines are labelled with their energies in keV. The closed circle (•), open circle (○) and triangle ($\triangle$) indicate γ rays from the β decay of ^{107}Sn, the isomeric transition of ^{107m}In and the β decay of ^{107g}In, respectively. The inset shows the low-energy part of the spectrum. The four lines without special symbol are assigned to the decay of ^{107}Sb.

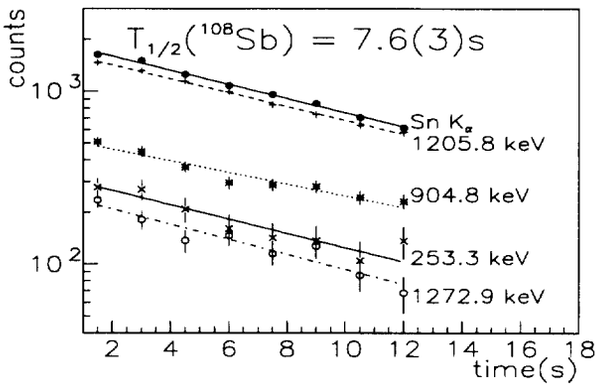

Figure 4: Decay characteristics measured for the Sn K_α X-rays and the most intense γ lines from the ^{108}Sb decay. The straight lines result from a single-component exponential fit to the experimental data.

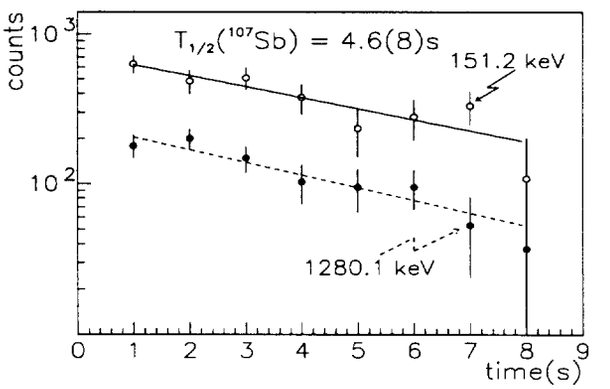

Figure 5: Decay characteristics measured for the most intense γ lines from the ^{107}Sb decay. The straight lines result from a single-component exponential fit to the experimental data.

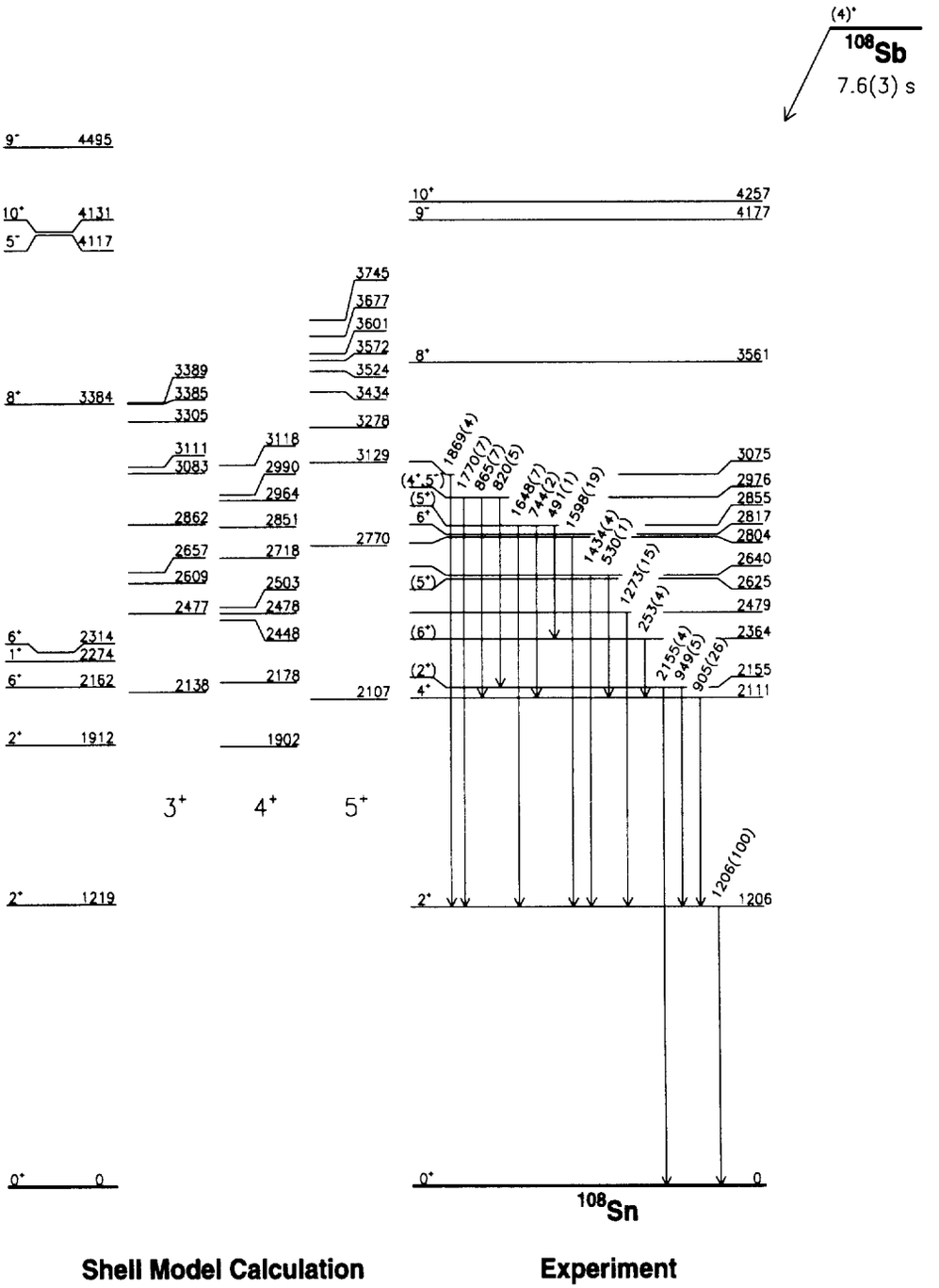

Figure 6: β-decay scheme of ^{108}Sb. The relative γ-ray intensities are given in brackets. For comparison with the shell model predictions, also selected high-spin states known from in-beam work are shown.

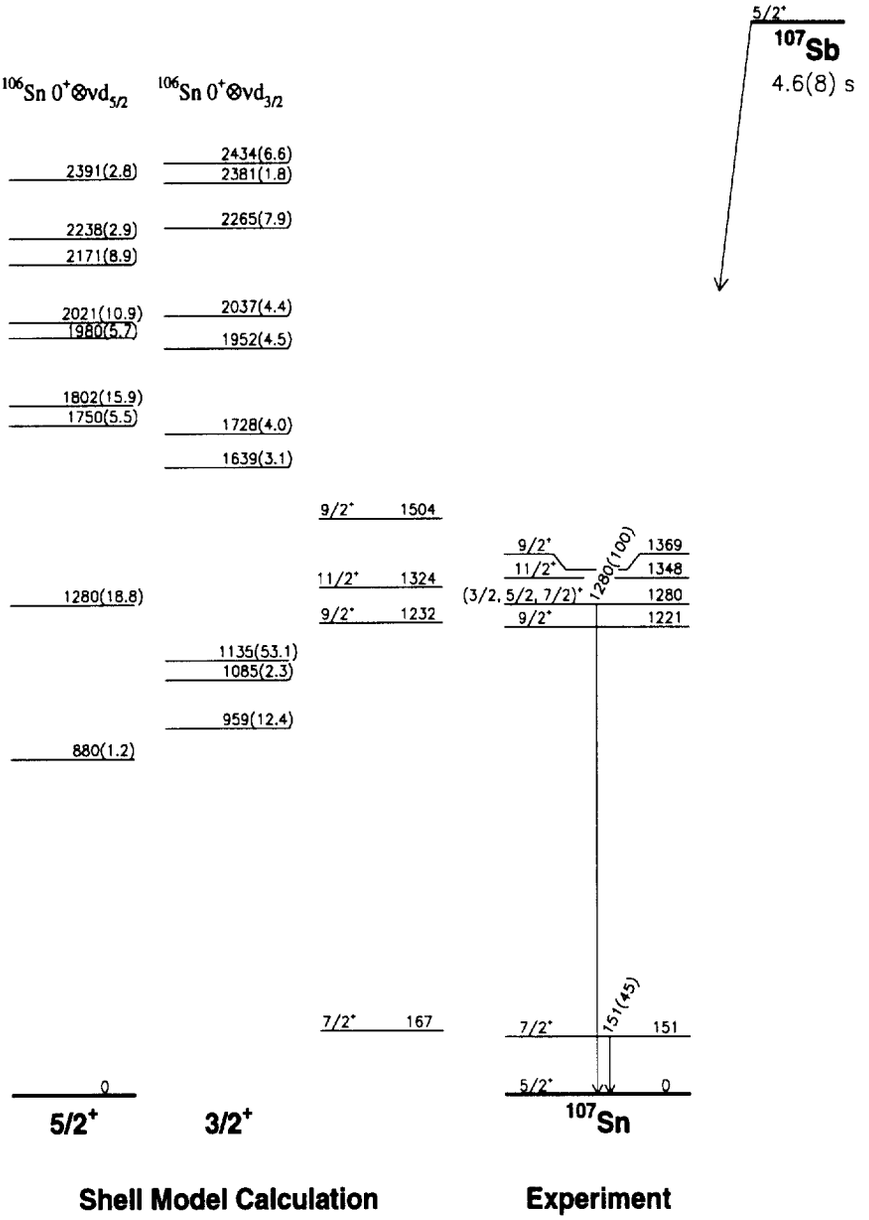

Figure 7: β-decay scheme of ^{107}Sb.

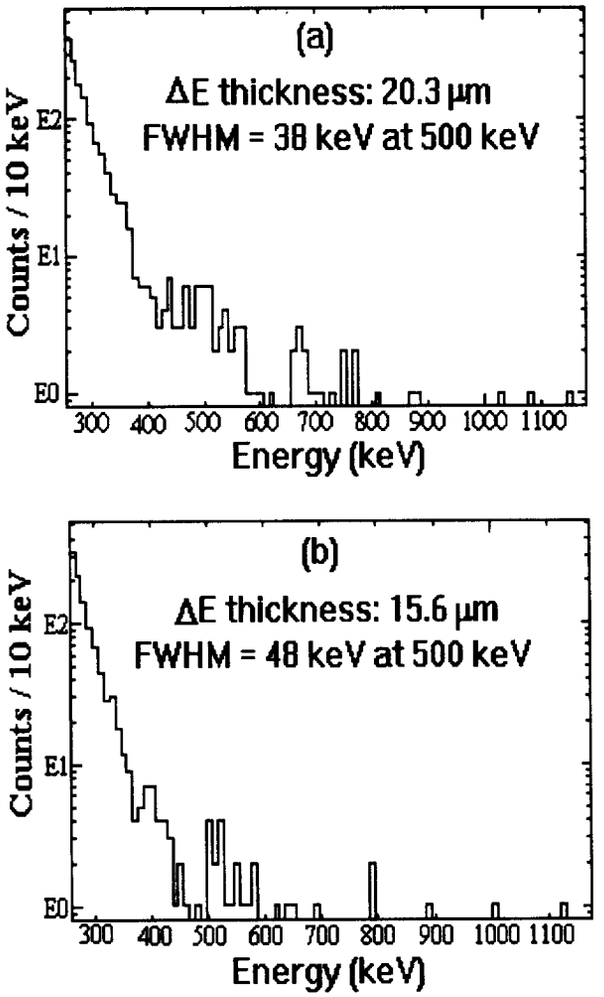

Figure 8: Energy spectra measured for mass 105 positron and proton activity. The data were accumulated by using the 20.3 μm thick (a) and 15.6 μm thick (b) ΔE detectors in anticoincidence with the respective E detectors. From the width of the 1051 keV proton line of ^{147}Tm, measured in a separate ^{92}Mo(^{58}Ni, p2n) experiment, the energy resolution at 500 keV is estimated to be 38 and 48 keV, respectively.